
# Site-Specific Management Zones Delineation Using Drone-Based Hyperspectral Imagery

**Hachem Agili[1], Karem Chokmani[1], Athyna Cambouris[2], Isabelle Perron[2], Jimmy Poulin[1]**

[1]Institut national de la recherche scientifique (INRS), Centre Eau Terre Environnement, 490, rue de la Couronne, Quebec City, QC, G1K 9A9, Canada; hachem.agili@ete.inrs.ca

[2]Agriculture and Agri-Food Canada, Quebec Research and Development Centre, 2560 Hochelaga Blvd., Quebec City, QC, G1V 2J3, Canada

***Abstract***

*Conventional techniques (e.g., intensive soil sampling) for site-specific management zones (MZ) delineation are often laborious and time-consuming. Using drones equipped with hyperspectral system can overcome some of the disadvantages of these techniques. The present work aimed to develop a drone-based hyperspectral imagery method to characterize the spatial variability of soil physical properties in order to delineate site-specific MZ. Canonical correlation analysis (CCA) was used to extract the most related wavelengths to the soil physical properties based on hyperspectral imagery. The selected spectral bands were 540, 704 and 816 nm. These bands were processed using an object-based image analysis (OBIA) technique to delineate two homogenous zones. A Student's t-test at the 5% significance level showed that these zones are statistically different in the physical soil properties. Also, a comparison between the extracted zones with the MZ obtained from the apparent soil electrical conductivity stratification yield very similar results. The results of this study suggested that MZ delineation using drone-based hyperspectral data can be a promising alternative to conventional techniques such as intensive soil sampling grid and soil proximal sensors.*

***Keywords:*** Management Zones, Drone, Hyperspectral Imagery, Soil Electrical Conductivity, CCA, OBIA

## Introduction

The delineation of site-specific management zones (MZ) is considered as a key practice to manage the precision agriculture operations. The identification of these zones within a field can be made using different techniques, such as yield maps and soil sampling (Cambouris et al. 2006). The last decades have seen a growing interest in proximal spectroscopy which can characterize soil properties, accurately and less expensive than conventional laboratory methods (Rossel et al. 2017). However, the majority of studies on the application of spectroscopy for soil properties analysis were carried out under laboratory controlled conditions using soil samples from the field (Bilgiliet al. 2011; Hermansen et al., 2017; Vašát et al., 2017). This method is as laborious and time-consuming as conventional soil property analysis due to the need to collect soil samples, and to analyze them separately. Using drones equipped with a light-weight hyperspectral system can overcome some of the disadvantages of the current soil proximal

spectroscopy techniques. Drones have the advantages of the ability to cover a large area in relatively short time. The use of a drone-based hyperspectral remote sensing to characterize soil would increase the speed and efficiency of the process while decreasing the labor and the lack of spatial coverage associated to proximal soil spectroscopy. Furthermore, drone-based hyperspectral imagery provides high spectral and spatial resolution images while facilitating large-scale monitoring and analysis (Adão et al. 2017). They allow many more measurements so that the data can adequately characterize the spatial and temporal variability of many soil properties. Finally, measurements are made directly in the field so that the data better represent the soil under field conditions. The main goal of the present work was to characterize the variability of the physical soil properties using drone-based hyperspectral data in order to delineate site-specific MZ.

## Material and methods

### Site characteristics

The study was conducted during 2015 and 2016 in a 12-ha sandy soil field located in Sainte-Catherine-de-la-Jacques-Cartier, near Quebec City, Canada (46°49'39"N, 71°40'38"W). The soil series was Pont-Rouge and was classified as Humo-Ferric Podzols (Soil Classification Working Group, 1998). The irrigated commercial potato (*Solanum tuberosum* L.) field was under *Russet Burbank* cultivar during both years.

### Soil sampling and apparent soil electrical conductivity measurements

Sampling of the soil surface layer (0-20 cm) was done in fall 2015 with an intensive triangular sampling grid of 12 points per hectare (Figure 1). Physical [clay, silt, sand content and soil organic matter (SOM)] soil properties were analyzed in laboratory using the pipette method (Kroetsch & Wang, 2007) to determine particle size distribution and by combustion method for the SOM (Skjemstad & Baldock, 2007). In addition, apparent soil electrical conductivity (ECa) was measured in fall 2016 over the field, following the potato harvest, using the Veris 3100 soil-mapping system (Veris technologies, KS, USA). This sensor measures the ECa in mS $m^{-1}$ to a depth between 0-30 cm ($EC_{30}$) and 0-100 cm ($EC_{100}$). Each soil ECa measurement was georeferenced using a GPS receiver which allows measuring the soil elevation. The descriptive statistics of the measured soil properties are shown in Table 1.

**Table 1. Descriptive statistics of the measured soil properties**

| | Mean | Std. Deviation | Coefficient of variation (%) |
|---|---|---|---|
| Clay (g $kg^{-1}$) | 74.0 | 14.0 | 19 |
| Silt (g $kg^{-1}$) | 130.0 | 51.0 | 39 |
| Sand (g $kg^{-1}$) | 796.0 | 59.0 | 7 |
| SOM (g $kg^{-1}$) | 61.0 | 10.0 | 16 |
| $EC_{30}$ (mS $m^{-1}$) | 1.7 | 0.6 | 35 |
| $EC_{100}$ (mS $m^{-1}$) | 1.4 | 0.7 | 50 |
| Elevation (m) | 151.8 | 2.5 | 2 |

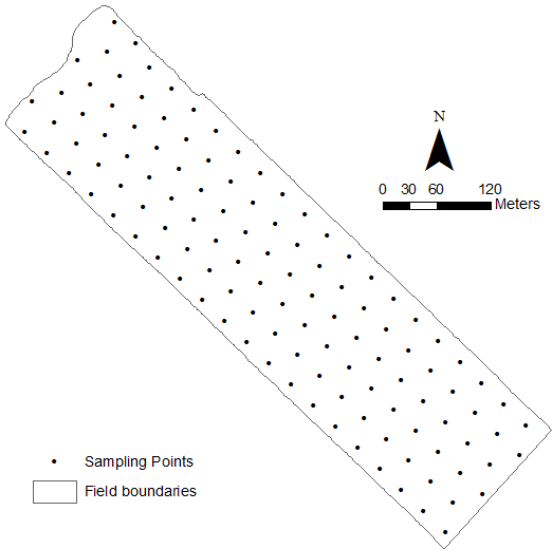


**Figure 1. Performed soil sampling grid in the experimental field**

## Drone-based hyperspectral imagery acquisition

A vertical take-off and landing (VTOL) hexacopter platform, model Hydra-12 (Altigator, Waterloo, Belgium), was used to collect hyperspectral data (Figure 2). This drone is equipped with 12 brushless motors powered by a set of two batteries and can lift until a 12-kg payload. The flight time can reach 25 minutes (without payload).The flights can be done manually or autonomously based on predefined waypoints.

**Figure 2. Drone used in the study (Hydra-12, Altigator)**

Two pushbroom hyperspectral imaging sensors manufactured by Resonon (Bozeman, MT, USA) were used. The first one, Pika II, collects data on 240 spectral bands in the visible-near-infrared (VNIR) spectral range (400-900 nm) with a 3-nm spectral resolution. The second one, Pika NIR, collects data on 148 spectral bands in the near-infrared (NIR) and the shortwave infrared (SWIR) spectral range (900-1700 nm) with 6-nm spectral resolution. Adding to the sensor, the hyperspectral imaging system includes an integrated GPS, an inertial navigation system (INS) unit (SBG Ellipse-N, SBG-Systems, Paris, France), a spectrometer (Ocean Optics, Largo, FL, USA) for measuring the downwelling irradiance spectrum and a flight computer. The whole hyperspectral imaging system weights approximately 5 kg for the Pika II sensor and 9 kg for the Pika NIR sensor.

The drone flights were carried out at 100-m altitude above ground level over bare soil field on

October 2016 after potato harvest. Three flights were completed for each hyperspectral sensor at 25% side-lap aiming to cover the whole field. The spatial resolutions of the collected hyperspectral data were 6 cm and 12 cm for the Pika II and the Pika NIR sensors, respectively.

### Hyperspectral data pre-processing

Digital numbers (DN) obtained with the hyperspectral imaging system were converted to radiance units using calibration coefficients provided by the manufacturer. A 12% reflectance calibration tarp was used to convert the radiance data to reflectance. The georectification procedure was carried out using Spectronon© software (developed by Resonon). The georectified datasets were then resampled to 1-m spatial resolution and a mosaic was created using the Seamless Mosaic functionality implemented in the ENVI 5.5 software (Harris Geospatial, Broomfield, CO, USA) (Figure 3).

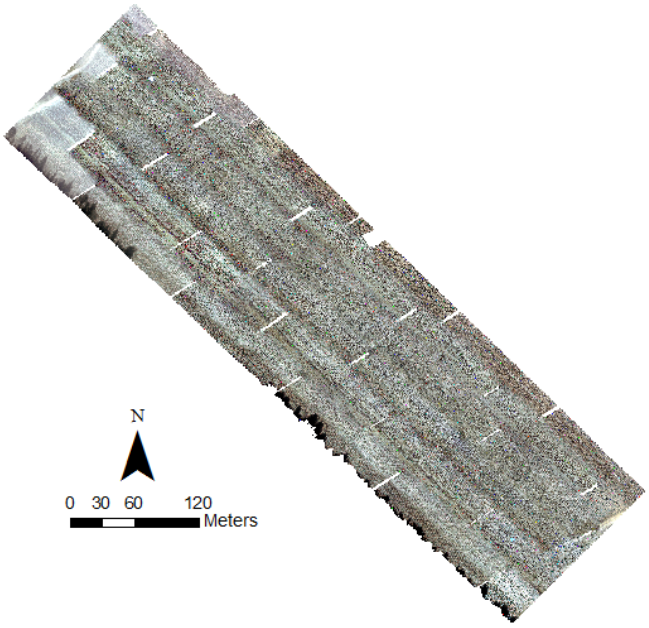


**Figure 3. True color hyperspectral data mosaic of the studied field (spectral bands: 640 nm, 550 nm, 460 nm)**

Two commonly used spectral preprocessing techniques were applied on the obtained hyperspectral mosaic: 1- Savitzky-Golay filter (Savitzky & Golay, 1964) which reduced the noise in the data and 2- Standard Normal Variate transformation (SNV) (Barnes et al. 1993) which removed arbitrary offsets and multiplicative effects (Jakob et al. 2017; Schläpfer & Richter, 2011; Žížala et al. 2017).

### Hyperspectral data processing

*Canonical Correlation Analysis*

Canonical Correlation Analysis (CCA) (Hotelling, 1936) is a multivariate statistical analysis technique which measures the linear dependency between two variable sets (e.g. **X** and **Y**) obtained from two separate data sources. The CCA aims to find two projection vectors *a* and *b* for **X** and **Y**, respectively such that the correlation (ρ) between the two new variable sets is maximized (Eq. (1)). In order to maximize this correlation, the derivatives of ρ with respect to *a* and *b* are set to zero.

$$\rho = corr\{a^T\boldsymbol{X}, b^T\boldsymbol{Y}\} = \frac{Cov\{a^T\boldsymbol{X}, b^T\boldsymbol{Y}\}}{\sqrt{var(a^T\boldsymbol{X})Var(b^T\boldsymbol{Y})}} = \frac{a^T\boldsymbol{C_{xy}}b}{\sqrt{a^T\boldsymbol{C_{xx}}a}\sqrt{b^T\boldsymbol{C_{xx}}b}} \quad \text{Eq. (1)}$$

Where $\mathbf{C_{xx}}$ is the dispersion matrix of the first set (**X**), $\mathbf{C_{yy}}$ is the dispersion matrix of the second set (**Y**) and $\mathbf{C_{xy}}$ is the covariance matrix between **X** and **Y**.

The output of CCA is two new variable sets **U** = $a^T$**X** and **V** = $b^T$**Y** having the same dimension *d*.

*d* is less than or equal the minimum dimension of the two original data sets. The first pair of canonical variates (CV) ($\mathbf{U}_1$, $\mathbf{V}_1$) has the maximum mutual information (the largest correlation). The canonical correlations decrease in the higher order CVs.

Using CCA allows to reduce the data dimensionality and to explain covariation between two sets of variables. The CCA is also useful in finding features that are important for explaining covariation between sets of variables.

In this study, before applying the CCA, the spectra corresponding to the soil sampling points were extracted from the hyperspectral data. So, the first group of variables (**X**) corresponds to the hyperspectral spectra (spectral variables) and the second group of variables (**Y**) correspond to the physical soil properties (soil variables) (Table 2). The clay was not included in the soil variables because it is related to the sand and silt information (i.e. redundant information). The output of the CCA is the canonical variables **U** (related to the spectral information) and **V** (related to the soil information). The most correlated spectral bands to the canonical variable **U** were extracted using the Pearson correlation (r) and then segmented using an Object Based Image Analysis.

**Table 2. Input variables for the CCA : X corresponds to the spectral variables and Y to the soil variables**

| | Spectral Variables (X) | | | | Soil Variables (Y) | | |
|---|---|---|---|---|---|---|---|
| | $\lambda_1$ | $\lambda_2$ | … | $\lambda_n$ | Sand | Silt | SOM |
| **Sample 1** | $x_{1,1}$ | $x_{1,2}$ | … | $x_{1,n}$ | $Y_{1,1}$ | $Y_{1,2}$ | $Y_{1,3}$ |
| **Sample 2** | $x_{2,1}$ | $x_{2,2}$ | … | $x_{2,n}$ | $Y_{2,1}$ | $Y_{2,2}$ | $Y_{2,3}$ |
| **…** | … | … | … | … | … | … | … |
| **Sample p** | $x_{p,1}$ | $x_{p,2}$ | … | $x_{p,n}$ | $Y_{p,1}$ | $Y_{p,2}$ | $Y_{p,3}$ |

$\lambda_i$ refers to reflectance value corresponding to wavelength I and p refers to the number of samples

*Object-based image analysis*

Object Based Image Analysis (OBIA) techniques allow to segment images into adjacent pixels with homogenous spectral information. These groups of pixels, called objects, are then used to do the classification (Peña et al. 2013). OBIA integrates spatial, spectral and contextual information in order to do the segmentation.

In this study, a multiresolution segmentation algorithm (MRSA) (Baatz & Schäpe, 2000) was used to segment the selected spectral bands in the previous step. This algorithm is implemented in eCognition Developer 8 software (Trimble GeoSpatial, Munich, Germany). MRSA is a bottom-up segmentation method based on a pairwise region-merging technique. Segmentation begins with single-pixel objects. These objects are merged through an iterative process with neighboring pixels until the object's internal heterogeneity exceeds the maximum allowed heterogeneity criterion set by the user through a scale parameter. This parameter controls of the size of the objects, the use of bigger scales results larger objects. The object homogeneity criterion is defined by a combination of spectral values (color) and geometrical properties (shape), based on compactness and smoothness criteria (Torres-Sánchez et al. 2015). After the segmentation procedure, the generated homogenous objects were classified according the mean spectral brightness of each object. A Student's *t*-test was used to determine whether there was a statistically significant difference between the obtained zones.

# Results and discussion

## CCA and wavelengths selection

Three CVs were obtained for each canonical variable (**U** and **V**) after the application of the CCA on the hyperspectral data and the studied physical soil properties. The three most correlated spectral bands to the canonical variable (**U**) were selected. These bands correspond to the wavelengths 540, 704 and 816 nm. The table below (Table 3) shows the correlation between the input variables (spectral and soil) and the obtained ones (**U** and **V**). The wavelengths 540 and 704 nm were significantly correlated to the silt and SOM content while the wavelength 816 nm was significantly correlated to the sand content.

**Table 3. Correlation (r) between physical soil properties, soil reflectance corresponding to selected bands and the canonical variables (U and V)**

| | | U | | | Soil properties | | |
|---|---|---|---|---|---|---|---|
| | | $U_1$ | $U_2$ | $U_3$ | Sand | Silt | SOM |
| **V** | $V_1$ | 0.87*** | 0.00 | 0.00 | -0.21* | 0.18 | -0.95*** |
| | $V_2$ | 0.00 | 0.82*** | 0.00 | 0.81*** | -0.92*** | 0.30** |
| | $V_3$ | 0.00 | 0.00 | 0.61*** | 0.54*** | -0.34*** | -0.05 |
| **Wavelength (nm)** | 540 | 0.71*** | 0.05 | -0.28** | -0.19* | 0.13 | -0.57*** |
| | 704 | 0.23* | 0.60*** | -0.11 | 0.32*** | -0.40*** | -0.04 |
| | 816 | -0.08 | -0.60*** | -0.11 | -0.42*** | 0.46*** | -0.08 |

* P-value < 0.05; ** P-value < 0.01; *** P-value < 0.001

The selected wavelengths are located in the VNIR spectral range. Similar results were obtained in many studies (Ben-Dor et al., 2002; Galvao & Vitorello, 1998; Krishnan et al. 1980; Nocita et al. 2013; Pinheiro et al. 2017). Pinheiro et al. (2017) suggested that the spectral range from 400-830 nm was the most relevant to characterize sand content. Galvao & Vitorellon (1998) and Nocita et al. (2013) found that the spectral range between 550-700 nm showed absorption features of SOM. Krishnan et al. (1980) found out that the spectral band 564 nm was useful to predict the SOM. Using an airborne hyperspectral imaging Ben-Dor et al. (2002) developed a model , using the 705-nm wavelength to predict SOM.

## Multiresolution Segmentation

The MRSA applied on the selected bands resulted in two homogeneous zones (Figure 4.a). The mean sand content in the first zone was 840 g $kg^{-1}$ and for the second one, it was 765 g $kg^{-1}$. The comparison of these zones with the MZs obtained from the application of the MRSA on the ECa showed similar results (Figure 4.b).

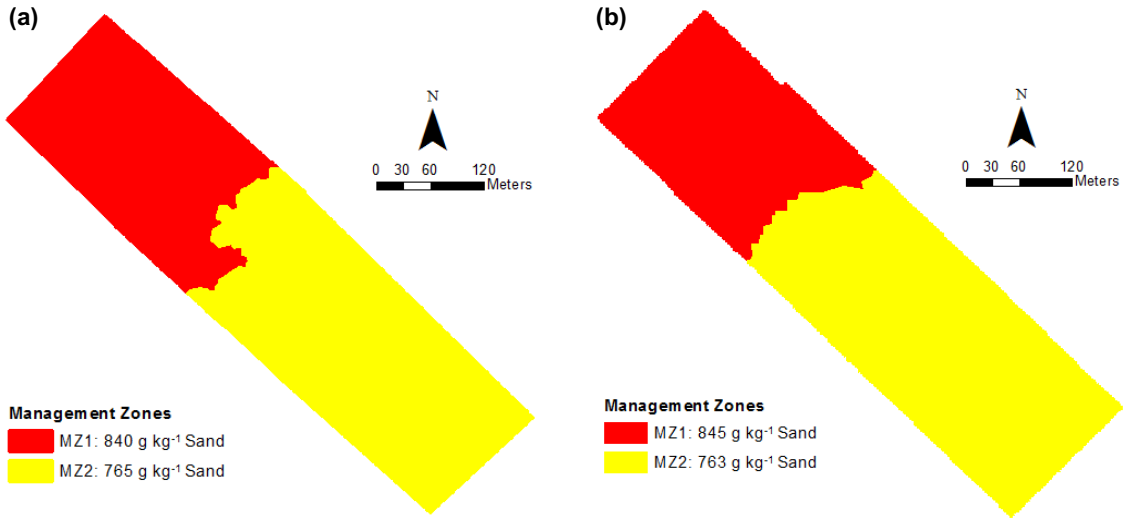


**Figure 4. Management Zones obtained using a) Drone-based hyperspectral data b) Soil electrical conductivity**

In order to validate the zones obtained from the segmentation of the drone-based hyperspectral data, a Student's *t*-test (p-value > 0.05) was conducted between the two zones along with the following soil properties: clay, silt, sand, SOM, $EC_{30}$, $EC_{100}$ and elevation. The obtained results show that there is a significant difference between the two delineated zones in the texture, SOM, $EC_{100}$ and elevation (Table 4).

**Table 4. Results of the Student *t*-test for MZ delineated using drone-based hyperspectral data**

| | Mean | | T-stat | P-value |
|---|---|---|---|---|
| | MZ1 | MZ2 | | |
| Clay (g $kg^{-1}$) | 68.1 | 77.8 | -4.0 | <0.001 |
| Silt (g $kg^{-1}$) | 91.9 | 156.9 | -8.5 | <0.001 |
| Sand (g $kg^{-1}$) | 840.0 | 765.2 | 8.7 | <0.001 |
| SOM (g $kg^{-1}$) | 56.8 | 63.8 | -4.0 | <0.001 |
| $EC_{30}$ (mS m-1) | 1.5 | 1.6 | -1.4 | >0.05 |
| $EC_{100}$ (mS m-1) | 1.5 | 1.2 | 4.2 | <0.001 |
| Elevation (m) | 150.8 | 153.2 | -7.6 | <0.001 |

## Conclusions

Drone-based hyperspectral imagery was used in this study to characterize the spatial variability of soil physical properties (sand, silt, SOM) in order to delineate site-specific MZ. Firstly, the CCA algorithm allowed the reduction of the dimensionality of hyperspectral data while maximizing the correlation with the soil properties data. The most relevant wavelengths were selected in the VNIR spectral range (540, 704, 816 nm). The OBIA conducted on the reflectance data corresponding to the selected wavelengths has shown a great potential for MZ delineation. The delineated zones were significantly different along with the texture, SOM, ECa and elevation. These results will be validated using drone-based hyperspectral imagery acquired during 2016 and 2017 above three other fields.

This study has shown that the soil surface reflectance can reflect the spatial variability of the physical soil properties at the field scale and serves to delineate MZ. The obtained results suggested that MZ delineation using drone-based hyperspectral data is a promising alternative to conventional techniques such as intensive soil sampling grid and soil proximal sensors.

### Acknowledgments

The research was supported by the project IA115317 funded by the Innov'Action program of Ministry of Agriculture, Fisheries and Food of Quebec and Agriculture and Agri-Food Canada.

## References

Adão, T., Hruška, J., Pádua, L., Bessa, J., Peres, E., Morais, R., & Sousa, J. (2017). Hyperspectral Imaging: A Review on UAV-Based Sensors, Data Processing and Applications for Agriculture and Forestry. *Remote Sensing*, *9*(11), 1110. http://doi.org/10.3390/rs9111110

Baatz, M., & Schäpe, A. (2000). Multiresolution Segmentation - an optimization approach for high quality multi-scale image segmentation. In *Angewandte Geographische Informationsverarbeitung XII. Beiträge zum AGIT-Symposium.* (pp. 12–23). Retrieved from http://www.ecognition.com/sites/default/files/405_baatz_fp_12.pdf

Barnes, R. J., Dhanoa, M. S., Lister, S. J., & Sd, Y. (1993). Correction to the description of Standard Normal Variate (SNV) and De-Trend (DT) Transformations in Practical Spectroscopy with Applications in Food and Beverage Analysis—2nd Edition. *J. Near Infrared Spectrosc*, *1*, 185–186. Retrieved from http://journals.sagepub.com.acces.bibl.ulaval.ca/doi/pdf/10.1255/jnirs.21

Ben-Dor, E., Patkin, K., Banin, A., Karnieli, A., Ben-Dor1, E., Patkin1, K., … Karnieli3, A. (2002). Mapping of several soil properties using DAIS-7915 hyperspectral scanner data -a case study over clayey soils in Israel Mapping of several soil properties using DAIS-7915 hyperspectral scanner data—a case study over clayey soils in Israel. *International Journal of Remote SensingOnline) Journal International Journal of Remote Sensing Int. J. Remote Sensing*, *236*(6), 143–1161. http://doi.org/10.1080/01431160010006962

Bilgili, A. V., Akbas, F., & van Es, H. M. (2011). Combined use of hyperspectral VNIR reflectance spectroscopy and kriging to predict soil variables spatially. *Precision Agriculture*, *12*(3), 395–420. http://doi.org/10.1007/s11119-010-9173-6

Cambouris, A. N., Nolin, M. C., Zebarth, B. J., & Laverdière, M. R. (2006). Soil management zones delineated by electrical conductivity to characterize spatial and temporal variations in potato yield and in soil properties. *American Journal of Potato Research*, *83*(5), 381–395. http://doi.org/10.1007/BF02872015

Galvao, L. S., & Vitorello, I. (1998). Role of organic matter in obliterating the effects of iron on spectral reflectance and colour of Brazilian tropical soils. *International Journal of Remote Sensing*, *19*(10), 1969–1979. http://doi.org/10.1080/014311698215090

Hermansen, C., Knadel, M., Moldrup, P., Greve, M. H., Karup, D., & de Jonge, L. W. (2017). Complete Soil Texture is Accurately Predicted by Visible Near-Infrared Spectroscopy. *Soil Science Society of America Journal*, *81*(4), 758. http://doi.org/10.2136/sssaj2017.02.0066

Hotelling, H. (1936). Relations Between Two Sets of Variates. *Biometrika*, *28*(3/4), 321. http://doi.org/10.2307/2333955

Jakob, S., Zimmermann, R., & Gloaguen, R. (2017). The Need for Accurate Geometric and Radiometric Corrections of Drone-Borne Hyperspectral Data for Mineral Exploration: MEPHySTo—A Toolbox for Pre-Processing Drone-Borne Hyperspectral Data. *Remote Sensing*, *9*(1), 88. http://doi.org/10.3390/rs9010088

Krishnan, P., Alexander, J. D., Butler, B. J., & Hummel, J. W. (1980). Reflectance technique for predicting soil organic

matter. *Soil Science Society of America Journal*, *44*(6), 1282–1285. http://doi.org/10.2136/sssaj1980.03615995004400060030x

Kroetsch, D., & Wang, C. (2007). Particle Size Distribution. In *Soil Sampling and Methods of Analysis, Second Edition* (pp. 713–725).

Nocita, M., Stevens, A., Noon, C., & Van Wesemael, B. (2013). Prediction of soil organic carbon for different levels of soil moisture using Vis-NIR spectroscopy. *Geoderma*, *199*, 37–42. http://doi.org/10.1016/j.geoderma.2012.07.020

Peña, J. M., Torres-Sánchez, J., Isabel De Castro, A., Kelly, M., & López-Granados, F. (2013). Weed Mapping in Early-Season Maize Fields Using Object-Based Analysis of Unmanned Aerial Vehicle (UAV) Images. *PLoS ONE*, *8*(10). http://doi.org/10.1371/journal.pone.0077151

Pinheiro, É., Ceddia, M., Clingensmith, C., Grunwald, S., & Vasques, G. (2017). Prediction of Soil Physical and Chemical Properties by Visible and Near-Infrared Diffuse Reflectance Spectroscopy in the Central Amazon. *Remote Sensing*, *9*(4), 293. http://doi.org/10.3390/rs9040293

Savitzky, A., & Golay, M. J. E. (1964). Smoothing and Differentiation of Data by Simplified Least-Squares Procedures. *Analytical Chemistry*, *36*, 1627–1639.

Schläpfer, D., & Richter, R. (2011). Spectral polishing of high resolution imaging spectroscopy data. *7th SIG-IS Workshop on Imaging Spectroscopy*, 1–7.

Skjemstad, J. O., & Baldock, J. A. (2007). Total and Organic Carbon. In *Soil Sampling and Methods of Analysis, Second Edition*.

Soil Classification Working Group. (1998). The Canadian System of Soil Classification. *NRC-CNRC*. Retrieved from http://sis.agr.gc.ca/cansis/publications/manuals/1998-cssc-ed3/cssc3_manual.pdf

Torres-Sánchez, J., López-Granados, F., & Peña, J. M. (2015). An automatic object-based method for optimal thresholding in UAV images: Application for vegetation detection in herbaceous crops. *Computers and Electronics in Agriculture*, *114*, 43–52. http://doi.org/10.1016/j.compag.2015.03.019

Vašát, R., Kodešová, R., Borůvka, L., Jakšík, O., Klement, A., & Brodský, L. (2017). Combining reflectance spectroscopy and the digital elevation model for soil oxidizable carbon estimation. *Geoderma*, *303*, 133–142. http://doi.org/10.1016/j.geoderma.2017.05.018

Viscarra Rossel, R. A., Lobsey, C. R., Sharman, C., Flick, P., & McLachlan, G. (2017). Novel Proximal Sensing for Monitoring Soil Organic C Stocks and Condition. *Environmental Science and Technology*, *51*(10), 5630–5641. http://doi.org/10.1021/acs.est.7b00889

Žížala, D., Zádorová, T., & Kapička, J. (2017). Assessment of soil degradation by erosion based on analysis of soil properties using aerial hyperspectral images and ancillary data, Czech Republic. *Remote Sensing*, *9*(1), 28. http://doi.org/10.3390/rs9010028